

See discussions, stats, and author profiles for this publication at: <https://www.researchgate.net/publication/46303353>

Shape-Controlled Synthesis of Single-Crystalline Nanopillar Arrays by Template-Assisted Vapor-Liquid-Solid Process

ARTICLE in JOURNAL OF THE AMERICAN CHEMICAL SOCIETY · OCTOBER 2010

Impact Factor: 12.11 · DOI: 10.1021/ja1052413 · Source: PubMed

CITATIONS

26

READS

37

10 AUTHORS, INCLUDING:



[Rehan Kapadia](#)

University of California, Berkeley

43 PUBLICATIONS 1,096 CITATIONS

[SEE PROFILE](#)



[Zhiyong Fan](#)

The Hong Kong University of Science and T...

117 PUBLICATIONS 6,032 CITATIONS

[SEE PROFILE](#)



[Ming C. Wu](#)

University of California, Berkeley

548 PUBLICATIONS 8,773 CITATIONS

[SEE PROFILE](#)



[Ali Javey](#)

University of California, Berkeley

219 PUBLICATIONS 14,833 CITATIONS

[SEE PROFILE](#)

Shape-Controlled Synthesis of Single-Crystalline Nanopillar Arrays by Template-Assisted Vapor–Liquid–Solid Process

Onur Ergen,^{†,‡,§} Daniel J. Ruebusch,^{†,‡,§} Hui Fang,^{†,‡,§} Asghar A. Rathore,^{†,‡,§} Rehan Kapadia,^{†,‡,§} Zhiyong Fan,^{†,‡,§} Kuniharu Takei,^{†,‡,§} Arash Jamshidi,^{†,‡} Ming Wu,^{†,‡} and Ali Javey^{*,†,‡,§}

Department of Electrical Engineering and Computer Sciences, University of California, Berkeley, California 94720, Berkeley Sensor and Actuator Center, University of California, Berkeley, California 94720, and Materials Sciences Division, Lawrence Berkeley National Laboratory, Berkeley, California 94720

Received June 15, 2010; E-mail: ajavey@eecs.berkeley.edu

Abstract: Highly regular, single-crystalline nanopillar arrays with tunable shapes and geometry are synthesized by the template-assisted vapor–liquid–solid growth mechanism. In this approach, the grown nanopillars faithfully reproduce the shape of the pores because during the growth the liquid catalyst seeds fill the space available, thereby conforming to the pore geometry. The process is highly generic for various material systems, and as an example, CdS and Ge nanopillar arrays with square, rectangular, and circular cross sections are demonstrated. In the future, this technique can be used to engineer the intrinsic properties of NPLs as a function of three independently controlled dimensional parameters - length, width and height.

In recent years, semiconductor nanowires (NWs) and nanopillars (NPLs) have been extensively explored for electronics, sensing, and energy applications.¹ Uniquely, their chemical and physical properties have been shown to exhibit a strong dependence on their dimensions, specifically the diameter and length, arising from various nanoscale phenomena.² Similarly, the cross-sectional shape and geometry of these nanostructures are expected to have an important effect on their properties. Yet, the controlled synthesis of single-crystalline NWs/NPLs with tunable shapes has not been well studied in part because the vapor–liquid–solid (VLS) growth mechanism often results in cylindrical structures as defined by the spherical shape of the catalytic seeds during the growth process.³ In some instances noncylindrical nanowires have been observed; however these structures are highly material and process dependent and, therefore, do not offer the control necessary to engineer nanowire shape for an arbitrary material system.⁴ Here, we utilize a template-assisted, VLS growth process⁵ for the fabrication of highly regular and single-crystalline NPL arrays with tunable shapes, such as square, rectangular, or circular cross sections, as defined by the shape and geometry of the templates. The process is applied for the synthesis of CdS and Ge NPLs, presenting a generic platform toward the controlled synthesis of nanostructures with tunable shape and geometry.

Porous anodized alumina membranes (AAMs)^{6,7} were used as the VLS templates (Figure 1), although the process scheme is generic for top-down fabricated templates as well. Briefly, the process scheme begins with the pretexture of an electrochemically polished 0.25 mm thick aluminum substrate (99.99%

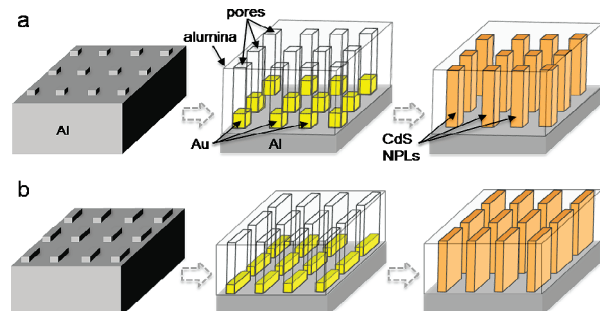


Figure 1. Process schematic for the template-assisted VLS synthesis of (a) square and (b) rectangular NPL arrays.

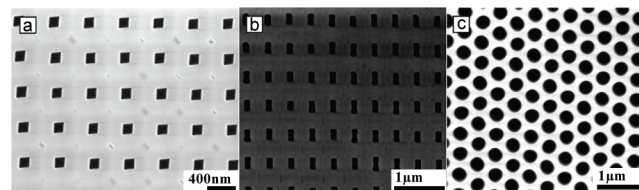


Figure 2. Top-view SEM images of the fabricated AAMs with (a) square, (b) rectangular, and (d) circular pores.

Alfa Aesar) using a straight-line silicon diffraction grating as the mold. A two-step imprinting process was utilized to define the Al surface morphology, followed by an anodization step (Figures S1–S2). By varying the angle between the two imprint orientations and the pitch of the gratings, different indentation shapes can be formed on the aluminum surface, resulting in pores with different cross-sectional shapes following the subsequent anodization step. This control is enabled since the indentation regions formed by the overlap of the two imprinting steps act as nucleation sites for the pore development due to a local increase in the rate of field-enhanced dissolution of the oxide.⁷ Figure 2 shows representative scanning electron microscope (SEM) images of the fabricated AAMs with square, rectangular, and circular pores with a pore depth of ~1.6 μm. The figure demonstrates that the pore shape is accurately controlled over large areas. The pore depth is also well manipulated by the anodization time. A current ramping technique was then used to thin the alumina barrier at the bottom of the pores (Figure S3c) in preparation for a subsequent Au electrodeposition step (Figure S3d). The detailed process procedures can be found in the Supporting Information.

The electrodeposited Au is then used as catalytic seeds for template-assisted VLS growth of NPLs (see Supporting Information).⁵ The process is generic for various NPL materials, and as an example, we demonstrate the shape-controlled synthesis of

[†] Department of Electrical Engineering and Computer Sciences, University of California.

[‡] Berkeley Sensor and Actuator Center, University of California.

[§] Lawrence Berkeley National Laboratory.

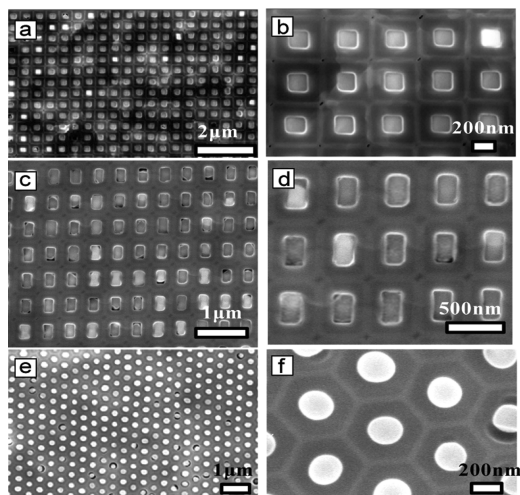


Figure 3. Top-view SEM images of highly ordered CdS NPLs with (a–b) square, (c–d) rectangular, and (e–f) circular cross sections, grown in AAM templates.

CdS (Figure 3) and Ge (Figure S4) NPLs. Figure 3 shows top-view SEM images of self-ordered pore arrays filled by indium-doped CdS NPLs with square ($\sim 165 \text{ nm} \times 165 \text{ nm}$) (Figure 3a), rectangular ($\sim 150 \text{ nm} \times 320 \text{ nm}$) (Figure 3b), and circular ($\sim 250 \text{ nm}$ diameter) (Figure 3c) cross-sectional shapes. The NPLs faithfully reproduce the shape of the pores because during the growth the liquid catalyst seeds fill the space available, thereby conforming to the pore geometry. To achieve this, sufficient gold must be deposited into the pores to ensure a complete filling of the cross-sectional pore area. If there is insufficient Au in the pores, spherical Au particles are formed during the growth, thereby resulting in the growth of cylindrical NPLs with diameters smaller than the width of the pores. Here, we have developed a simple geometrical argument to conservatively estimate the minimum thickness of Au necessary to achieve shaped controlled synthesis. A detailed discussion of this model can be found in the Supporting Information. The resulting relationships are

$$T_{\text{Au}} = \left(\frac{4}{3}\right)R; T_{\text{Au}} = \frac{(x\pi\sqrt{2})}{3}; T_{\text{Au}} = \left(\frac{\pi}{6xy}\right)(y^2 + z^2)^{3/2}$$

for the circular, square, and rectangular pores respectively, where T_{Au} is the Au thickness at the bottom of the pores, R is the radius of the circular pores, x is the width of the square pores, and y and z are the cross-sectional width and length of the rectangular pore. From our pore dimensions, we obtain a minimum Au thickness of ~ 167 , 222 , and 480 nm for circular, square, and rectangular pores respectively. We note that in the template-assisted VLS mechanism, successful growth can be achieved as long as the gold thickness is more than the minimum values explained above (Figure S6), beyond which it has minimal effect on the growth.

The shape controlled synthesis process described here is also compatible with top-down fabricated templates. In this regard, we have fabricated fin-like Ge single-crystals (length $\sim 1.5 \mu\text{m}$, width $\sim 380 \text{ nm}$, height $\sim 2 \mu\text{m}$) on Si/SiO₂ substrates (Figure S5), demonstrating the potential utility of the scheme for heterogeneous and/or three-dimensional electronics on Si substrates. The rectangular nanopores used as templates were fabricated by electron beam lithography and dry etching of a $\sim 2 \mu\text{m}$ thick SiO₂ layer (Figure S5). Notably, a result of the growth process is that the NPL surfaces incorporate any roughness present on the pore sidewalls. The

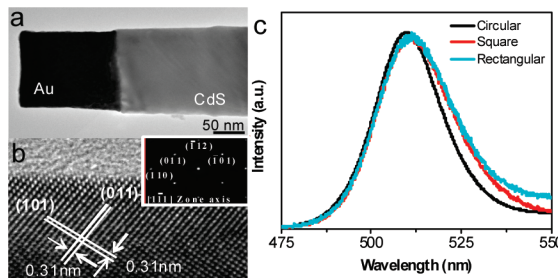


Figure 4. (a–b) TEM images of square-shaped CdS NPL, depicting its single crystalline structure. (c) PL spectra of square, rectangular, and circular CdS NPLs.

reliable production of extremely smooth pore sidewalls is needed, which is an inherent advantage of the AAM templates as compared to nanopores fabricated using top-down etching methods.

The crystal structure and materials quality of the shape-controlled CdS NPLs were characterized by transmission electron microscopy (TEM) and photoluminescence (PL) spectroscopy. The low magnification TEM image of a square-shaped CdS NPL with the corresponding electron diffraction pattern shows the single crystalline nature of the as-grown structures (Figure 4a). The Au catalytic seed is clearly depicted in the TEM image, which is a signature of the VLS growth. The high-resolution TEM image depicts the lattice fringes and preferred [110] growth direction (Figure 4a). The observed lattice spacing is the same as that for circular CdS NPLs.^{5a} The PL spectra of the CdS NPLs (Figure 4b) illustrate band emission at $\sim 512 \text{ nm}$ for different shape NPLs. There is no peak shift as compared to the previously reported bulk CdS value,⁸ which is expected since the scale of the explored NPLs is still beyond the Bohr radius of bulk CdS ($\sim 5 \text{ nm}$). In the future, NPLs with dimensions on the order of the Bohr radius can be synthesized and characterized to observe quantization effects and the corresponding divergence in the properties of NPLs of differing shapes. Successful scaling of this templated growth process presents significant challenges, including the formation of $\sim 5 \text{ nm}$ pores with sharp corners and good wetting properties.

In summary, a versatile route toward the controlled synthesis of single crystalline NPL arrays with tunable shapes is demonstrated by a template-assisted VLS growth mechanism. The ability to control the cross-sectional geometry of NWs in addition to their dimensions provides yet another degree of control in exploring novel phenomena at the nanoscale and designing materials with the desired properties and functionalities.

Acknowledgment. This work was funded by BSAC and MDV. The synthesis part was supported by an LDRD from LBL. A.J. acknowledges support from World Class University program.

Supporting Information Available: Detailed information about AAM fabrication, alumina barrier thinning, NPL growth, and the minimal Au thickness required for a successful growth. SEM images after various process steps and for Ge NPL growth are also shown. This material is available free of charge via the Internet at <http://pubs.acs.org>.

References

- (a) Lieber, C. M.; Wang, Z. L. *MRS Bull.* **2007**, *32*, 99–104. (b) Javey, A. *ACS Nano* **2008**, *2*, 1329–1335. (c) Yang, P.; Fardy, M.; Yan, R. *Nano Lett.* **2010**, *10*, 1529.
- (a) Ford, A. C.; Ho, J. C.; Chueh, Y.-L.; Tseng, Y.-C.; Fan, Z.; Guo, J.; Bokor, J.; Javey, A. *Nano Lett.* **2009**, *9*, 360. (b) Ma, D. D. D.; Lee, C. S.; Au, F. C. K.; Tong, S. Y.; Lee, S. T. *Science* **2003**, *299*, 1874. (c) Tian, B.; Xie, P.; Kempa, T. J.; Bell, D. C.; Lieber, C. M. *Nat. Nanotechnol.* **2009**, *4*, 824.

- (3) (a) Wagner, R. S.; Ellis, W. C. *Appl. Phys. Lett.* **1964**, *4*, 89. (b) Kodambaka, S.; Tersoff, J.; Reuter, M. C.; Ross, F. M. *Science* **2007**, *316*, 729.
- (4) (a) Kuykendall, T.; Pauzauskie, P.; Lee, S.; Zhang, Y.; Goldberger, J.; Yang, P. *Nano Lett.* **2003**, *3*, 1063. (b) Wagner, V.; Parillaud, O.; Buhlmann, J.; Illegems, M. *J. Appl. Phys.* **2002**, *92*, 1307.
- (5) (a) Fan, Z.; Razavi, H.; Do, J.; Moriwaki, A.; Ergen, O.; Chueh, Y.-L.; Leu, P. W.; Ho, J. C.; Takahashi, T.; Reichertz, L. A.; Neale, S.; Yu, K.; Wu, M.; Ager, J. W.; Javey, A. *Nat. Mater.* **2009**, *8*, 648. (b) Fan, Z.; Kapadia, R.; Leu, P.; Zhang, X.; Chueh, Y.-L.; Takei, K.; Yu, K.; Jamshidi, A.; Rathore, A.; Ruebusch, D.; Wu, M.; Javey, A. *Nano Lett.* **2010**, ASAP (DOI: 10.1021/nl1010788). (c) Lew, K. K.; Reuther, C.; Carim, A. H.; Redwing, J. M.; Martin, B. R. *J. Vac. Sci. Technol. B* **2002**, *20*, 389.
- (6) (a) Masuda, H.; Fukuda, K. *Science* **1995**, *268*, 1466. (b) Masuda, H.; Asoh, H.; Watanabe, M.; Nishio, K.; Nakao, M.; Tamamura, T. *Adv. Mater.* **2001**, *13*, 189.
- (7) (a) Parkhutik, V. P.; Shershulsky, V. I. *J. Phys. D: Appl. Phys.* **1992**, *25*, 1258. (b) Lee, W.; Ji, R.; Ross, C. A.; Goselle, U.; Nielsch, K. *Small* **2006**, *2*, 978.
- (8) Perna, G.; Capozzi, V.; Ambrico, M.; Augelli, V.; Ligorio, T.; Minafra, A.; Schiavulli, L.; Pallara, M. *Thin Solid Films* **2004**, *453*, 187.

JA1052413

Shape-Controlled Synthesis of Single-Crystalline Nanopillar Arrays by Template-Assisted Vapor-Liquid-Solid Process

Onur Ergen,^{†,‡,§} Daniel J. Ruebusch,^{†,‡,§} Hui Fang,^{†,‡,§} Asghar A. Rathore,^{†,‡,§} Rehan Kapadia,^{†,‡,§}
Zhiyong Fan,^{†,‡,§} Kuniharu Takei,^{†,‡,§} Arash Jamshidi,^{†,‡} Ming Wu^{†,‡} and Ali Javey*,^{†,‡,§}

[†]*Department of Electrical Engineering and Computer Sciences, University of California at Berkeley, Berkeley, CA 94720*

[‡]*Berkeley Sensor and Actuator Center, University of California at Berkeley, CA 94720*

[§]*Materials Sciences Division, Lawrence Berkeley National Laboratory, Berkeley, CA 94720*

*Email: ajavey@eecs.berkeley.edu

Supporting Information

AAM Template Fabrication

By using a two-step imprinting process with a 90° rotation and a Si mold with 416.6 nm period (208 nm line width), square-shaped pores (pitch 420nm and size 150nm) can be readily achieved during the subsequent anodization step. On the other hand, a 60° rotation enables the fabrication of circular pores. Similarly, rectangular-shaped pores are formed by using two different Si grating molds, for instance, with 416.6 nm and 555.5 nm period, and a 90° rotation between the two imprints. The applied pressure during the imprinting process was $\sim 1 \times 10^4 \text{ Ncm}^{-2}$. Following the double imprint step, the Al substrates were anodized in 1:100:200 H₃PO₄: Ethylene Glycol:H₂O under 166 V DC bias for 2h at 10°C. The appropriate anodization voltage had to be chosen such that the periodicity of the pores matched the pitch of the imprints by using the well-known pitch-to-voltage ratio of $\sim 2.5 \text{ nm/V}$. In the case of the two-pitch double imprinting process, the voltage was chosen to match the smaller pitch (i.e., 416.6 nm). Upon completion of the anodization step, a low-angle ion milling was performed in order to planarize the top surface of the alumina membrane (Fig. S3).

Alumina Barrier Thinning

The alumina barrier thinning procedure is a current controlled room temperature anodization in 0.2 M H₃PO₄ with a starting voltage of $\sim 164 \text{ V}$, followed by a periodic halving of the anodization current to induce decay of the measured anodization voltage until the final voltage of 4.6 V is reached. This step is followed by a quick 10 second etch of the membrane in 5% wt H₃PO₄ at 53°C to wet the pores before gold deposition. Using a potentiostat (SG 300, Gamry Instruments) and a gold electrodeposition solution (Technic gold 25 ES), Au was electrochemically deposited into the pores with a 60 Hz sinusoidal voltage. During this 20 min process, the voltage amplitude was raised from 3.5 to 6.5 V in order to uphold the reaction with

peak current density of 8 to 10 mA cm⁻². Note that this barrier thinning procedure is critical for uniform electrodeposition of Au at the bottom of the pores.

NPL Syntheses

Indium-doped CdS NPLs were grown in a 1-inch quartz tube solid source chemical vapor deposition furnace with two separate resistive heating zones. The vapor-liquid-solid growth required ~0.5 g of CdS powder (99.999%, Alfa Aesar) as the source, heated to 700°C in the first heating zone (upstream). The indium supply (~225 mg In pellet) was placed immediately upstream of the CdS source using a different quartz boat. The Au deposited AAM sample was placed in the second zone (downstream) and heated to 550°C with 5 min sample annealing time, while a hydrogen gas flow of 50 sccm was introduced. The chamber pressure was kept constant at 15 torr. The growth was carried out for 30 minutes, after which the furnace was shut down and allowed to cool rapidly. A subsequent ion milling (1kV Ar⁺, ~80° incident angle, and with a water cooled sample chuck) was performed to remove the surface covered CdS layer so that only the NPLs within the pores remained.

Ge NPLs were also grown by the Au catalyzed VLS mechanism. After Au electrodeposition inside the pores, the samples were placed in the middle of a single zone furnace followed by heating to 285°C in an H₂ ambient. After reaching 285°C, GeH₄ (10%, diluted in H₂) was flown at 12 sccm and a pressure of 40 torr. Total growth time was 20 min. After the growth, the samples were initially mechanically polished to partially remove the surface covered film and then ion milled for 1h (1kV Ar⁺, 80° incident angle with a water cooling chuck).

We note that after NPLs are grown out of the pores, the Au catalytic seeds often split into multiple smaller particles as they are no longer confined by the template walls. This in effect

results in the growth of a nanowire forest and even thin film on the surface of AAM. The purpose of ion milling after the NPL growth is to remove this undesired layer. In the future, this may be avoided by either exploring a vapor-solid-solid growth process by changing the catalytic seed material and/or optimizing the growth condition and time such that the NPLs are grown only up to the surface of the pores.

Au Thickness Calculation

We have developed a simple geometrical model for estimating the Au thickness required in the pores to achieve good pore filling (i.e., shape controlled synthesis). Here, we estimate that upon initiation of NPL growth the liquid Au will take the shape of a sphere due to the poor wetting of Au on alumina surfaces (Fig. S6b,f)¹. In order to ensure complete pore filling, the unconfined Au sphere must have sufficient volume to circumscribe the pore cross section. The cross section of the Au sphere and square pore are depicted in Fig. S6c and S6g for insufficient and sufficient Au thicknesses, respectively. Equating the volume of the solid Au at the bottom of the pore and the liquid Au sphere, we can obtain a simple relationship between the pore dimensions and the required Au thickness to ensure good filling as presented in the main text. This basic analysis can be easily extended to pores with rectangular and circular cross sectional shapes.

It is important to note that we have purposefully made simplifying assumptions that overestimate the Au thickness. The contact angle of Au on the aluminum oxide will not be 180 degrees, and thus assuming a liquid Au sphere overestimates the Au requirement. Further, by equating the solid and liquid Au volume we neglect expansion of the Au due to temperature, phase change, and incorporation of CdS during growth. Finally, in this analysis we ignore the Au deposited into the pore sub-channels and focus only on the Au thickness above the top of the

sub-channels necessary for successful shape controlled growth. Plugging in our pore dimensions we obtain a minimum Au thickness of ~167 nm, 222 nm, and 480 nm for circular, square, and rectangular pores respectively. Our experimental observations indicate that this process is easily reproduced and not extremely sensitive to Au thickness, especially for thicknesses exceeding our stated minimum values. These simple expressions are meant strictly as a basic guideline.

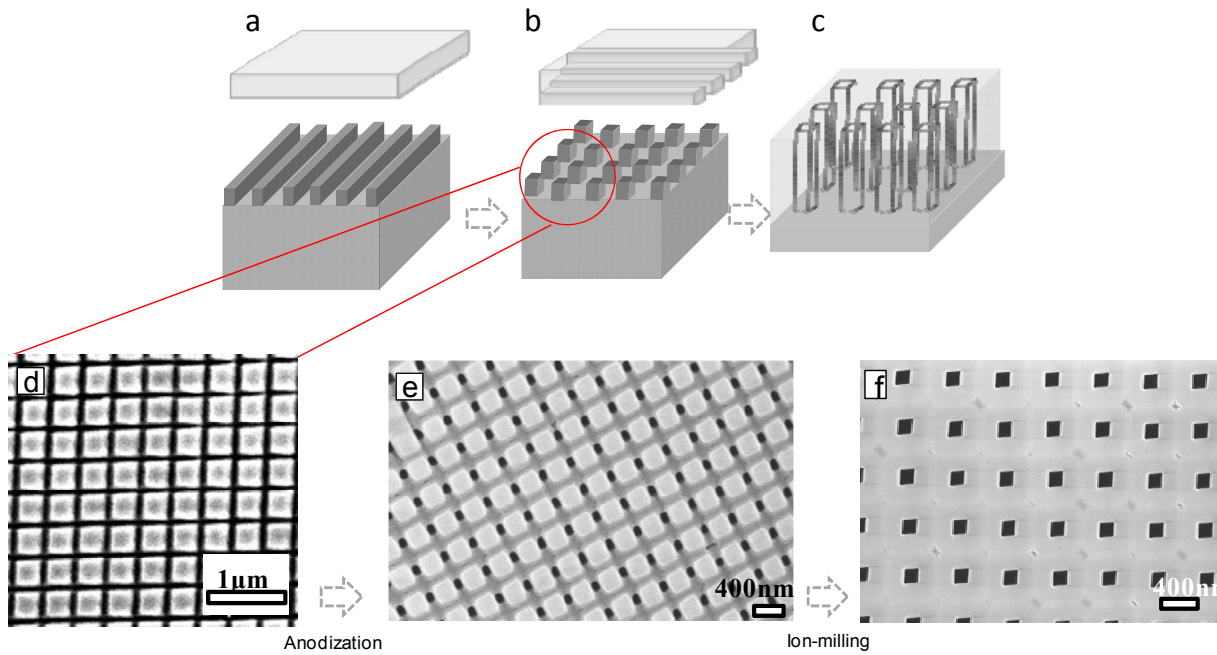


Figure S1. Fabrication of AAM with square-shaped nanopores. Schematic illustration of texturing the Al surface by a 90° double imprint process using identical pitch Si grating (a-b), and the subsequent anodization process which results in square-shaped pore formation (c). SEM images of a pre-textured Al surface after double imprinting with a Si grating (pitch 416.6 nm) (d), followed by anodization (e), and ion milling to planarize the surface (f). Cross-sectional images of the pore arrays before and after ion milling are shown in Figure S3.

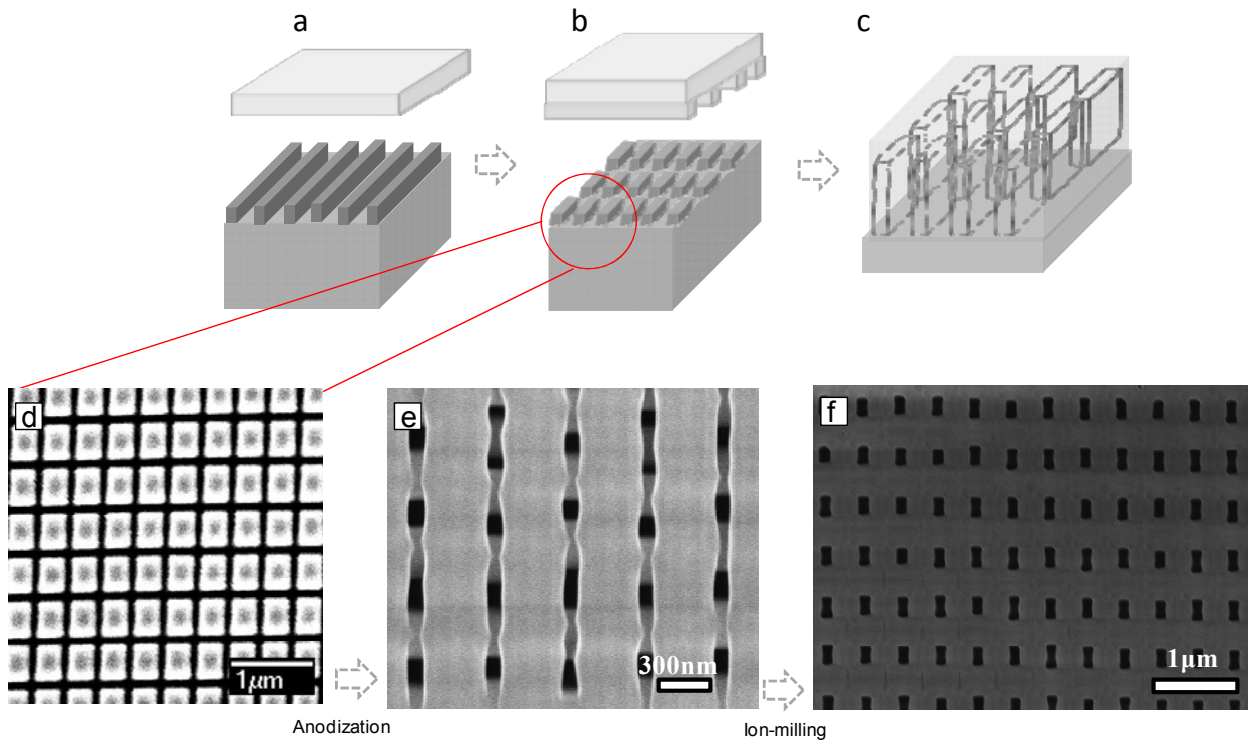


Figure S2. Fabrication of AAM with rectangular nanopores. Schematic illustration of texturing the Al surface by a 90° double imprint process using Si gratings with two different pitch (a-b), and the subsequent anodization process which results in pores with rectangular cross-sections (c). SEM images of a pre-textured Al surface after double imprinting with two different Si gratings (pitch 416.6nm and 555.5 nm) (d), followed by anodization (e), and ion milling to planarize the surface (f).

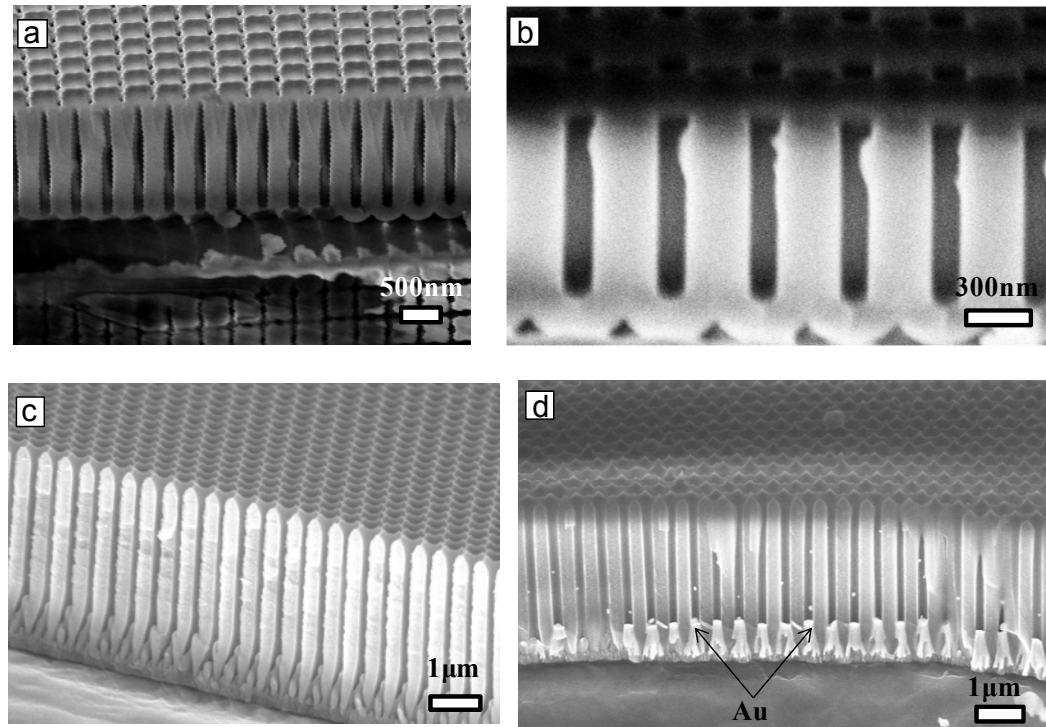


Figure S3. Cross sectional SEM images of a fabricated AAM with square-shaped pores (a) before and (b) after ion milling. The SEM image in a, clearly shows that the pore shape and geometry near the surface (the first ~500 nm) is different than that of the rest of the pore, arising from the textured surface used for anodization. This ~500 nm thick layer is removed by ion milling to enable pore arrays with uniform depth profiles. Note that the alumina barrier layer at the bottom of each pore is clearly evident in b. Cross sectional SEM images of a fabricated 3.3 μ m thick AAM after (c) barrier thinning and (d) Au electrodeposition steps. Au thickness above the top of the pore subchannels roughly matches our basic geometrical model presented in the main text.

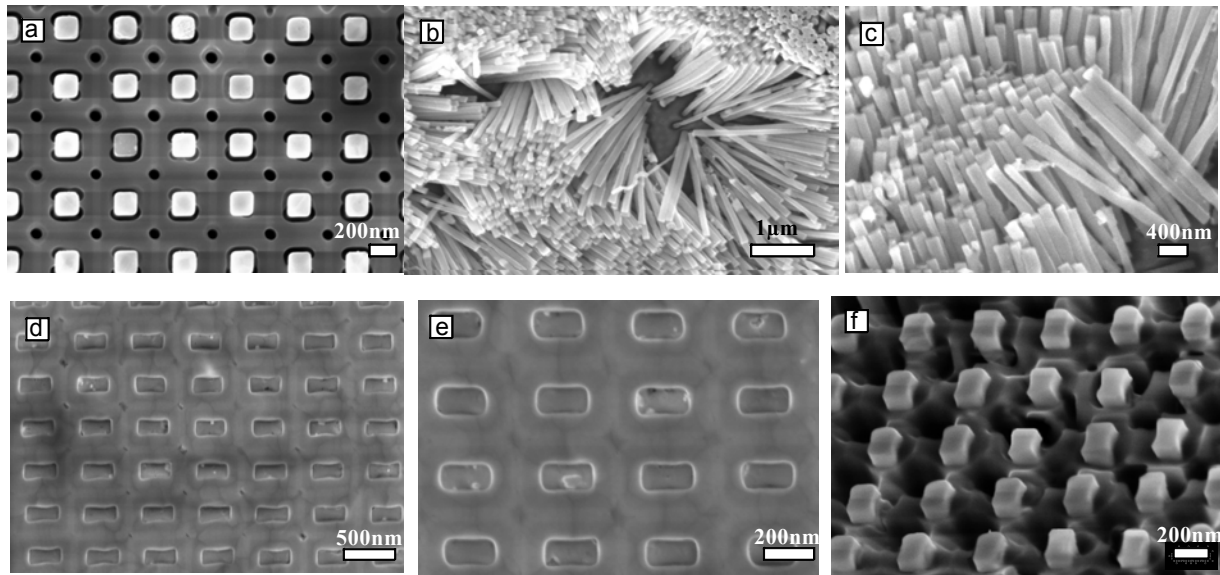


Figure S4. SEM images of shape-controlled Ge NPLs. (a) Square-shaped Ge NPLs after 10 min, 1M NaOH etch to partially etch the alumina membrane and expose the NPLs in order to enhance the contrast for SEM imaging. Note that after the NaOH etch, parasitic pores are formed in the alumina membrane arising from a difference in the local etch rate of alumina. (b-c) After full etching of the AAM bonded with epoxy on glass in NaOH, leaving behind the unsupported NPLs. (d-e) Rectangular-shaped Ge NPLs. (f) Rectangular-shaped Ge NPLs after 40min NaOH etch on Al substrate which allows us to see sharp edges.

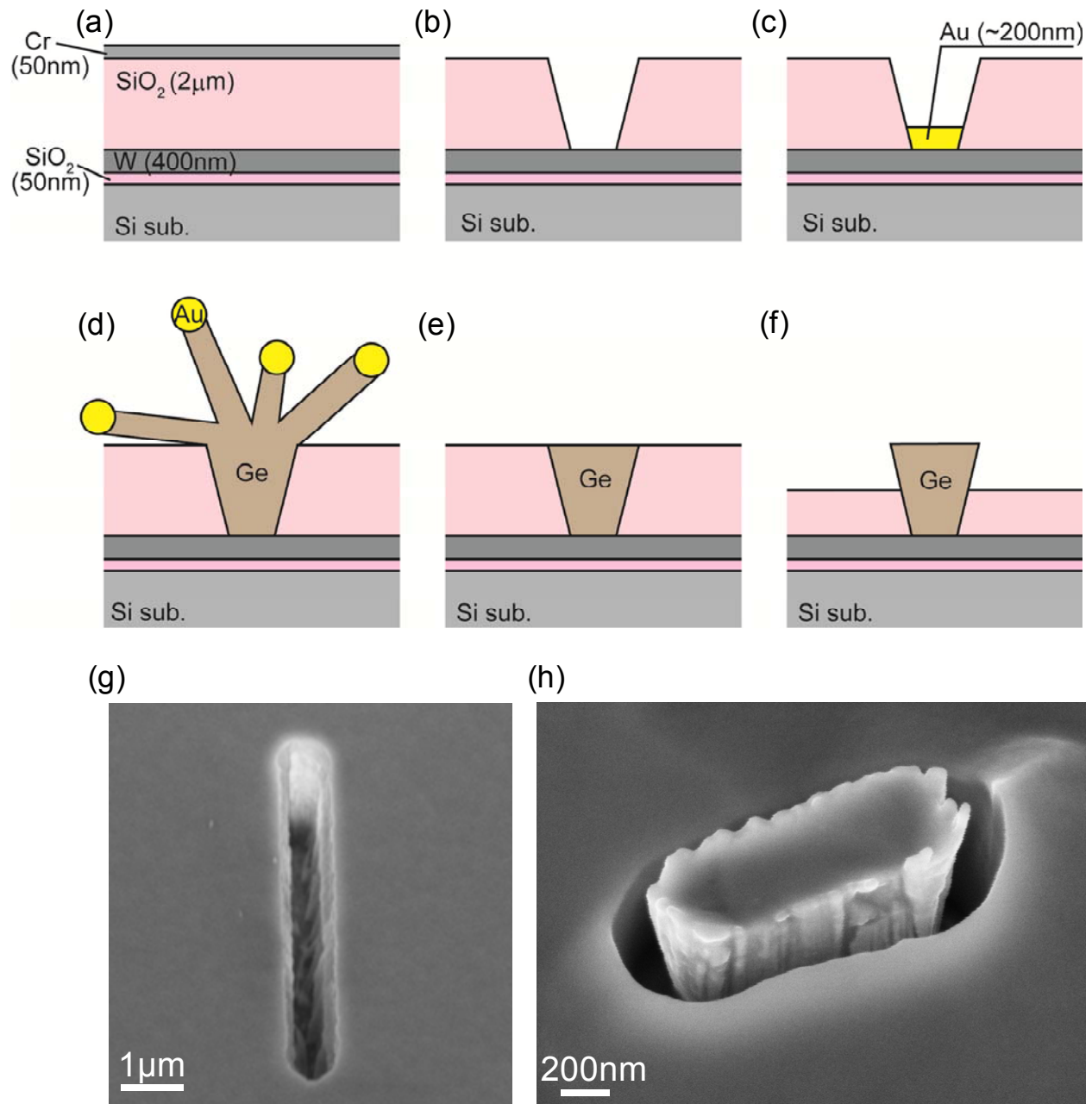


Figure S5. Schematic illustration and SEM images of Ge NPLs grown inside of top-down fabricated templates using a Au-catalyzed VLS process. (a-f) Fabrication process schematic. Si/SiO₂(50nm)/W(400nm)/SiO₂(2μm)/Cr (50 nm) substrates are patterned by e-beam lithography and wet etching of the Cr layer. Patterned Cr is then used as the hard mask for the reactive ion etching of SiO₂ (b). W electrode is used to electrochemically deposit a ~200 nm Au layer at the

bottom of each pore (c). Ge NPLs are then grown, initially confined by the shape of the pore template followed by splitting of the catalytic seeds once the NPLs reach the surface (d). Ion milling is then performed to remove the unwanted surface Ge layer (e). SiO₂ template is partially wet etched in HF to expose the NPLs (f). (g) SEM image of a rectangular nanopore fabricated by the described procedure and corresponding to the step shown in part (b). (h) Angled-view SEM of a Ge NPL grown by using the Au catalyzed VLS process inside a rectangular pore, corresponding to the step shown in part (f). Note that since the pores are fabricated by the top-down processing, they exhibit severe surface roughness. The grown NPLs inherit the surface roughness of the initial templates.

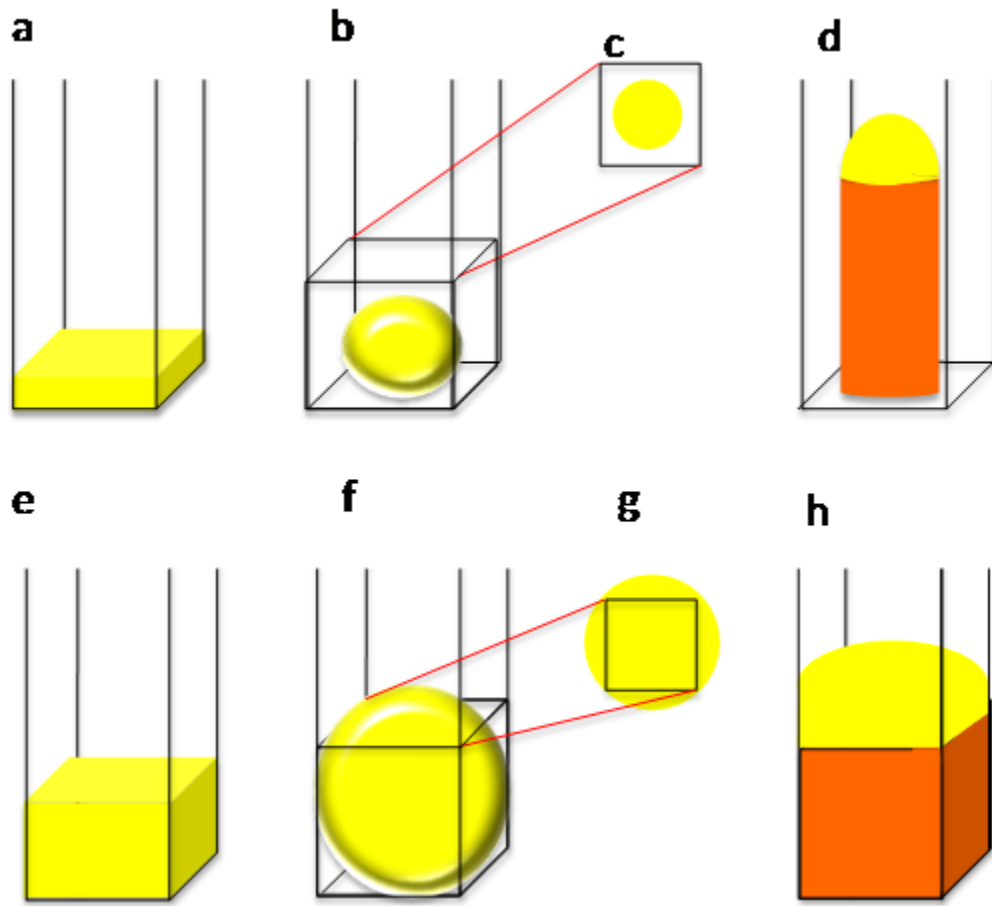


Figure S6. Schematic illustration of Au thickness requirement to achieve good pore filling for shape controlled growth. (a-d) Simplified growth illustration for insufficient Au thickness. Upon heating the solid Au with a thickness below the minimal requirement (a), it melts to form a sphere (b) with a diameter smaller than the dimensions of the pore cross section (c). The resulting growth is a cylindrical NPL (d) similar to growth processes without AAM templates. (e-h) Simplified growth illustration for sufficient Au thickness (e). The melted Au sphere (f) is large enough to circumscribe the pore cross section (g), thus the pore completely confines the dimensions of the liquid Au. The resulting growth is effectively shape controlled by the pore (h).

References

¹ Lee, J.; Ishimura, H.; Tanaka, T.; *Scripta Materialia* **2006**, 54, 1369.